

Submillisecond AMPA Receptor-Mediated Signaling at a Principal Neuron–Interneuron Synapse

Jörg R. P. Geiger,* Joachim Lubke,† Arnd Roth,‡
Michael Frotscher,† and Peter Jonas*

*Physiologisches Institut der Universität Freiburg

†Anatomisches Institut der Universität Freiburg

D-79104 Freiburg

Federal Republic of Germany

‡Max-Planck-Institut für medizinische Forschung

D-69120 Heidelberg

Federal Republic of Germany

Summary

Glutamatergic transmission at a principal neuron–interneuron synapse was investigated by dual whole-cell patch-clamp recording in rat hippocampal slices combined with morphological analysis. Evoked EPSPs with rapid time course (half duration \approx 4 ms; 34°C) were generated at multiple synaptic contacts established on the interneuron dendrites close to the soma. The underlying postsynaptic conductance change showed a submillisecond rise and decay, due to the precise timing of glutamate release and the rapid deactivation of the postsynaptic AMPA receptors. Simulations based on a compartmental model of the interneuron indicated that the rapid postsynaptic conductance change determines the shape and the somatodendritic integration of EPSPs, thus enabling interneurons to detect synchronous principal neuron activity.

Introduction

The neuronal network of the hippocampus operates via synaptic interactions between glutamatergic principal neurons (PNs) and GABAergic interneurons (INs). Although INs numerically represent only \sim 10% of the neuronal population, they control the activity of the entire hippocampal circuitry by feed-forward and feedback inhibition (reviewed by Freund and Buzsáki, 1996). In addition, INs are thought to participate in the generation of oscillatory network activity (reviewed by Jefferys et al., 1996).

Excitatory postsynaptic potentials (EPSPs) generated at PN–IN synapses are the trigger signals that initiate feed-forward or feedback inhibition. The duration and the amplitude of the EPSPs define whether postsynaptic neurons operate as integrators or coincidence detectors of synaptic events (Shadlen and Newsome, 1994; König et al., 1996; Reyes et al., 1996), or as relays mediating spike-to-spike transmission (Miles, 1990; Zhang and Trussell, 1994b; Borst et al., 1995). Previous studies indicated that EPSPs generated at PN–IN synapses in the hippocampus and neocortex show a shorter duration and larger amplitude than EPSPs at PN–PN synapses (Lacaille et al., 1987; Miles, 1990; Gulyás et al., 1993; Thomson et al., 1993; Debanne et al., 1995), suggesting that INs may operate as coincidence detectors

or relays. The factors that determine the time course and amplitude of the EPSP include the location and number of synaptic contacts, the passive properties of the IN membrane, and the time course and amplitude of the postsynaptic conductance change (Rall, 1967; Jack and Redman, 1971). The main pre- and postsynaptic factors that determine the time course of the postsynaptic conductance change, however, have remained controversial at glutamatergic synapses.

Asynchrony of quantal release from presynaptic boutons contributes to both the rise and decay time course of the excitatory postsynaptic current (EPSC; Diamond and Jahr, 1995; Isaacson and Walmsley, 1995). At some glutamatergic synapses, the transmitter is cleared from the synaptic cleft very rapidly by diffusion and glutamate transporters, implying that deactivation of the postsynaptic receptors primarily shapes the EPSC decay (Clements et al., 1992; Colquhoun et al., 1992; Hestrin, 1993; Jonas et al., 1993; Silver et al., 1996). At other synapses, transmitter clearance appears to be slower, and the EPSC decay may approach the desensitization time course (Trussell et al., 1993; Barbour et al., 1994; Menerick and Zorumski, 1995). Multivesicular release, either from the same presynaptic site (Tong and Jahr, 1994a) or from different, closely spaced sites (Trussell et al., 1993), could further prolong the time course of the glutamate concentration in the synaptic cleft.

Deactivation and desensitization of the glutamate receptors of the L- α -amino-3-hydroxy-5-methyl-4-isoxazolepropionate type (AMPA) are the main postsynaptic factors that may shape the EPSC time course. Both deactivation and desensitization kinetics of AMPARs are regulated by the subunit composition (Mosbacher et al., 1994; Geiger et al., 1995). Molecular analysis by single-cell RT-PCR (reverse transcription polymerase chain reaction) revealed that INs and PNs differ markedly in the expression of AMPAR subunits (GluR1 to 4 or GluR-A to -D; Jonas et al., 1994; Geiger et al., 1995) and splice versions (flip and flop; Geiger et al., 1995; Lambolez et al., 1996). This raises the possibility that AMPAR subunit gene expression in postsynaptic neurons differentially controls the kinetics of synaptic transmission at PN–IN and PN–PN synapses.

Here, we examine excitatory synaptic transmission at a prototypic PN–IN synapse in the hippocampus between granule cells (GCs) and basket cells (BCs) of the dentate gyrus, by combining dual whole-cell patch-clamp recording with morphological analysis. The location of the synapses at basal dendrites electrotonically close to the BC soma allowed us to dissect pre- and postsynaptic contributions to the postsynaptic conductance change by recording EPSCs in the voltage-clamp configuration. Our results indicate that the time course of the evoked EPSC at the GC–BC synapse is very fast, shaped mainly by the high synchrony of transmitter release and the rapid time course of AMPAR deactivation. In addition, we show that the rapid time course of the postsynaptic conductance change controls both the shape and the temporal summation of somatic EPSPs, and thus may be a main determinant of the input–output relation of GABAergic interneurons.

Results

Unitary EPSPs Generated at Principal Neuron–Interneuron Synapses in the Hippocampus

Excitatory synaptic transmission between synaptically coupled GCs and BCs of the dentate gyrus was investigated in acute hippocampal slices at 32°C–36°C using the patch-clamp technique. A representative example of an evoked EPSP recorded in the current-clamp configuration is shown in Figure 1A. Evoked EPSPs in the BC had a mean amplitude ranging from 0.7–3 mV (Table 1) and showed a very rapid time course. The half duration of the EPSPs, which describes the overall kinetics, was 3.7 ± 0.2 ms (Figure 1B; Table 1). The mean value of the 20%–80% rise time of the average evoked EPSP was 488 ± 68 μ s. Evoked EPSPs decayed biexponentially in four of seven pairs and with a single exponential in the remaining pairs. The amplitude-weighted mean of the decay time constants of the average EPSPs was 4.6 ± 0.3 ms (Table 1). Hence, the kinetics of evoked EPSPs generated at the GC–BC synapse were more than 5-fold

faster than those of EPSPs generated at synapses between PNs in the hippocampus and neocortex (Miles and Wong, 1986; Markram et al., 1997).

The rapid time course of the EPSP largely prevented the temporal summation of multiple EPSPs evoked by repetitive activation of the presynaptic GC (Figure 1C). Following a train of three action potentials separated by 20 ms intervals, the amplitude of the second and the third evoked EPSP was markedly reduced in comparison to that of the first, indicating the absence of temporal summation and, in addition, the presence of paired-pulse depression at the GC–BC synapse (Figure 1C).

The time course of EPSPs generated at excitatory synapses on PNs is shaped significantly by the passive membrane properties of the postsynaptic neuron (Rall, 1967; Jack and Redman, 1971; Miles and Wong, 1986; Markram et al., 1997). To assess the passive membrane properties of the BC, de- or hyperpolarizing current pulses of small amplitude were applied, and the apparent membrane time constant (τ_d) was determined by linear fitting of the late portion of the logarithmically plotted voltage transients (Figure 1D). The mean value

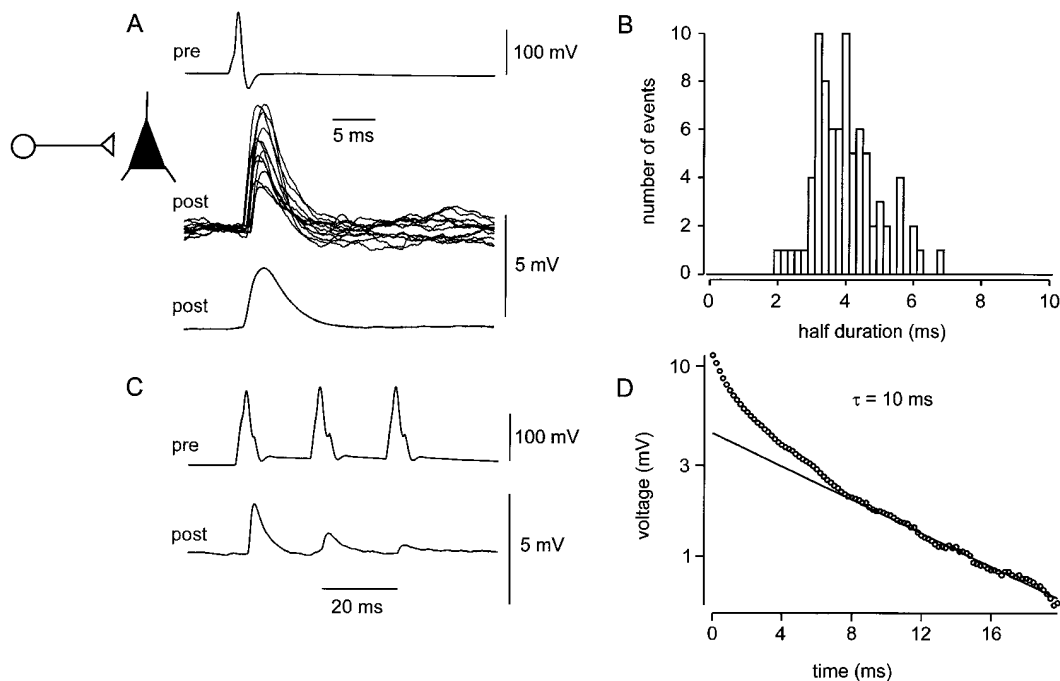


Figure 1. Rapid Time Course of Unitary EPSPs Generated at the GC–BC Synapse

(A) Simultaneous recording from a presynaptic GC and a postsynaptic BC in a hippocampal slice at 34°C. Both cells were held in the whole-cell current-clamp recording configuration. The top trace shows an action potential in the presynaptic GC. Individual evoked EPSPs in the postsynaptic BC are shown superimposed in the middle traces. The bottom trace shows the average evoked EPSP (average of 89 individual traces).

(B) A histogram of the half duration of individual evoked EPSPs. The mean value of the half duration was 4.4 ms in this pair.

(C) EPSPs evoked by three action potentials separated by 20 ms intervals. The top trace shows action potentials in the presynaptic GC; the bottom trace shows the average evoked EPSPs in the BC (average of 90 single traces).

(D) Semi-logarithmic plot of the voltage transient at the beginning of a long hyperpolarizing current pulse in the BC (100 pA). The apparent membrane time constant, estimated by linear fit of the voltage waveform between 10 and 20 ms after the beginning of the pulse, was 10 ms. Similarly, the apparent membrane time constant estimated from the voltage transient at the end of a long depolarizing current pulse was 9.5 ms in this BC (40 pA current, 5 mV voltage change, comparable to the amplitude of the largest EPSPs; see Table 1).

The data shown in (A), (B), and (D) were from the same GC–BC pair; the resting potential of the BC was -62 mV. The data in (C) were from a different pair. The pipette solution for the postsynaptic neuron was KCl intracellular solution.

of τ_0 in BCs obtained using depolarizing pulses was 8.4 ± 0.7 ms (5 pairs; Table 1), at least 3-fold faster than τ_0 in hippocampal PNs (Spruston and Johnston, 1992) but ~ 2 -fold slower than the amplitude-weighted mean decay time constant of the EPSP ($P < 0.05$). These results indicate that the membrane properties of the postsynaptic BC can only partly account for the fast EPSP, and may imply that GC–BC synapses differ from excitatory synapses between PNs in their functional characteristics or location.

Glutamate Receptors Mediating Evoked EPSPs and EPSCs

The rapid kinetics of the EPSP suggest that only fast AMPARs, but no N-methyl-D-aspartate receptors (NMDARs), contribute to synaptic events at the GC–BC synapse. To clarify the contribution of AMPARs and NMDARs to the synaptic events, we examined the effects of the selective AMPAR antagonist 6-cyano-7-nitroquinoxaline-2,3-dione (CNQX) and the selective NMDAR antagonist D-2-amino-5-phosphonopentanoic acid (D-AP5; Figure 2). At holding potentials of -70 mV (close to resting potential) and -52 mV (slightly below the threshold for action potential initiation), the time course of the average evoked EPSP was unaffected by addition of $50 \mu\text{M}$ D-AP5 to the extracellular solution

(Figure 2A). In addition, the decay kinetics of the EPSP showed no voltage dependence in the early phase and only a minimal voltage dependence in the late phase, which was slightly slower at -52 mV than at -70 mV (Figure 2A). This suggests that little, if any, amplification of EPSPs by voltage-activated Na^+ channels occurs (Stuart and Sakmann, 1995; Traub and Miles, 1995). Whereas the EPSP was insensitive to D-AP5, it was almost entirely blocked by further addition of $5 \mu\text{M}$ CNQX to the extracellular solution (Figure 2B). As the experimental conditions should favor NMDAR activation ($10 \mu\text{M}$ extracellular glycine), this may suggest that NMDARs are either absent from the postsynaptic membrane of GC–BC synapses or blocked by extracellular Mg^{2+} in the subthreshold range of membrane potentials.

To distinguish between these possibilities, EPSCs were recorded in the voltage-clamp configuration at -70 mV and $+50$ mV. At -70 mV, the average evoked EPSC was rapidly rising and decaying, and was completely blocked by $5 \mu\text{M}$ CNQX (Figure 2C). At $+50$ mV, a dual-component EPSC was observed. Whereas the fast component was unaffected by $100 \mu\text{M}$ D-AP5, the slow component was blocked (Figure 2C). The mean ratio of the NMDAR-mediated conductance change (determined at $+50$ mV) and the AMPAR-mediated conductance change (determined at -70 mV, assuming a reversal

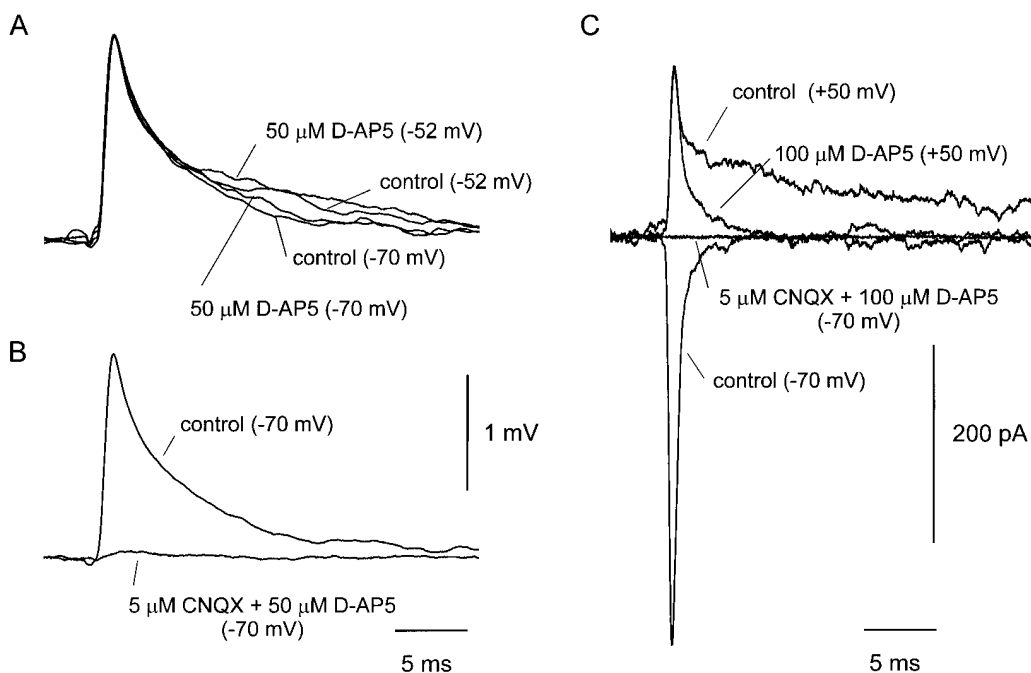


Figure 2. Contribution of AMPARs and NMDARs to Unitary EPSPs and EPSCs

(A) Unitary average EPSPs at -70 mV and -52 mV, in physiological extracellular solution and in the presence of $50 \mu\text{M}$ D-AP5, as indicated. Average EPSPs were obtained from 150–250 individual traces and normalized to the peak amplitude of the control EPSP at -70 mV (see B). Note that the unitary EPSP was slightly slower at -52 mV than at -70 mV, but that D-AP5 did not affect the time course.

(B) Unitary EPSPs at -70 mV, in physiological solution and in the presence of $5 \mu\text{M}$ CNQX and $50 \mu\text{M}$ D-AP5.

(C) Contribution of AMPARs and NMDARs to the evoked EPSC at -70 mV and $+50$ mV, in physiological extracellular solution and in the presence of $100 \mu\text{M}$ D-AP5 and $100 \mu\text{M}$ D-AP5 + $5 \mu\text{M}$ CNQX, respectively, as indicated. Average EPSCs were obtained from 24–80 individual traces.

The data in (A) and (B) are from the same GC–BC pair; the data in (C) are from a different pair. The extracellular solution contained $10 \mu\text{M}$ glycine in all experiments. The pipette solution for the postsynaptic neuron was K-gluconate (A and B) or Cs-gluconate intracellular solution (C).

Table 1. Summary of Functional and Morphological Properties of the Glutamatergic GC-BC Synapse

	mean ± SEM [range] (n)
EPSPs	
half duration individual EPSPs	3.7 ± 0.2 ms [3.1–4.7] (7)
20–80% rise time average EPSP	488 ± 68 μs [323–852] (7)
amplitude-weighted decay τ average EPSP ^a	4.6 ± 0.3 ms [3.1–5.5] (7)
peak amplitude average EPSP (excluding failures ^b)	2.1 ± 0.3 mV [0.7–3.0] (7)
EPSCs	
latency average of EPSC ^c	892 ± 74 μs [708–1350] (9)
20–80% rise time of average EPSC	249 ± 15 μs [159–313] (9)
decay τ of average EPSC	772 ± 91 μs [473–1302] (9)
peak amplitude average EPSC (excluding failures ^b)	315 ± 58 pA [153–578] (9)
20–80% rise time of quantal EPSC ^d	143 ± 16 μs [102–171] (4)
decay τ of quantal EPSC ^d	367 ± 29 μs [306–418] (4)
peak amplitude of quantal EPSC ^d	160 ± 31 pA [104–249] (4)
percentage of failures (2 mM Ca ²⁺ , 1 mM Mg ²⁺) ^e	20 ± 6% [0–52] (12)
decay τ of release period ^e	298 ± 15 μs [255–323] (4)
g_{NMDAR}/g_{AMPA} ^f	39 ± 6% [25–66] (6)
decay τ of NMDAR-mediated EPSC component	19.4 ± 3.1 ms [11.6–27.1] (6)
Morphological Properties	
number of putative GC-BC contacts	2.9 ± 0.2 [2–4] (8)
axonal distance from GC soma to contact ^g	118 ± 11 μm [30–241] (23)
standard deviation of axonal distance ^{g,h}	39 ± 13 μm [3–76] (6)
dendritic distance from contact to BC soma ^g	70 ± 8 μm [7–147] (23)
standard deviation of dendritic distance ^{g,h}	37 ± 3 μm [29–48] (6)
diameter of GC hilar collateral boutons	1.2 ± 0.1 μm [0.5–2] (25)
diameter of mossy fiber boutons in CA3	3.1 ± 0.2 μm [2.7–5.7] (25)
Passive Properties of BC	
apparent membrane time constant BC ⁱ	8.4 ± 0.7 ms [6.7–10.6] (5)
input resistance BC ⁱ	56 ± 9 MΩ [33–76] (5)

All measurements were taken at 34°C.

^a In 4 of 7 pairs, the decay of the EPSP was biexponential (mean $\tau_1 = 1.7$ ms; $\tau_2 = 9.3$ ms), whereas it was monoexponential in the remaining pairs (mean $\tau = 4.4$ ms). The amplitude-weighted average EPSP decay time constant was determined as the mean of τ , τ_1 , and τ_2 from individual experiments, τ_1 and τ_2 being weighted with their respective fractional amplitude contributions (mean values, 0.48 and 0.52).

^b A trace was classified as failure when the amplitude was less than three times the standard deviation of the preceding baseline current.

^c The latency was measured from the maximum of the first derivative of the presynaptic GC action potential to the beginning of the EPSC.

^d Quantal EPSCs were from two pairs in which the probability of transmitter release was reduced by decreasing the Ca²⁺/Mg²⁺ concentration ratio from 2 to 0.5 (44% and 64% failures), and from two additional pairs in which release probability was low from the beginning (40% and 43% failures). Assuming binomial release statistics with four release sites, a proportion of failures of 45% would imply that 72% of events were single quanta. In addition, events that showed a nonmonotonous rise or decay (indicating multiquantal release) were excluded from the analysis.

^e The release probability distribution was obtained from the first latency histogram using the method of Barrett and Stevens (1972). The decay τ of the release period was determined by fitting the decay of the corrected histogram data with a single exponential function.

^f The mean ratio of NMDAR-mediated chord conductance (determined at +50 mV) and AMPAR-mediated chord conductance (determined at -70 mV), assuming a reversal potential of 0 mV.

^g Axonal and dendritic distances were measured from the GC soma to the putative synaptic contact and from the BC soma to the putative synaptic contact.

^h The standard deviation of axonal and dendritic distance of different putative synaptic contacts of the same connection. Only pairs with three or four putative synaptic contacts were used.

ⁱ The apparent membrane time constant was determined in the current-clamp configuration using long depolarizing current pulses (100–500 ms, 20 or 40 pA). The voltage waveform at the end of the pulse was plotted logarithmically, and the portion between 10–20 ms was fit by linear regression. The amplitude of the depolarizations was comparable to that of the largest EPSPs.

^j The input resistance was determined in the voltage-clamp configuration from the current response to a 2 mV pulse.

potential of 0 mV) was 39% ± 6% (6 pairs, Table 1). These results indicate that the EPSC generated at GC-BC synapses is mediated by both AMPARs and NMDARs (Bekkers and Stevens, 1989; McBain and Dingledine, 1992), but that the contribution of NMDARs to the EPSP at subthreshold voltages is minimal, due to a voltage-dependent block by Mg²⁺.

Number and Location of Putative GC-BC Synaptic Contacts

The location of synaptic contacts is a main factor that shapes the EPSP time course (Rall, 1967). We therefore

analyzed the morphological properties of eight synaptically connected GC-BC pairs that were filled with biocytin during recording. A photomicrograph and the corresponding camera lucida drawing of a representative GC-BC pair are shown in Figures 3 and 4. In this particular pair, three putative excitatory synaptic contacts were found, established between the hilar collaterals of the GC axon and the basal dendrites of the BC (Figure 3B). In the pairs analyzed, between 2 and 4 putative synaptic contacts were identified (Figure 4B; Table 1). All putative synaptic contacts were established between collaterals of the GC axon and basal dendrites of the BC within the

hilar region. The mean axonal length (measured from the GC soma to the putative synaptic contact) was 118 μm (range, 30–241 μm ; Figure 4C), and the mean dendritic length (measured from the BC soma to the putative synaptic contact) was 70 μm (range, 7–147 μm ; Figure 4D). Putative synaptic contacts of the same connection were always formed on different dendritic branches of the BC. The diameters of the presynaptic boutons of the hilar collaterals were relatively small (~ 1 μm ; Table 1), much smaller than those of mossy fiber boutons established by the GC main axon (Table 1). These results show that the GC–BC synapse is a distributed synapse comprised of multiple contacts and that a subset of synaptic contacts is located close to the soma of the postsynaptic BC.

In all reconstructed GC–BC pairs, the axon of the BC originated at the soma and projected into the granule cell layer; the extensive arborization of the axon was mainly confined to this layer (Figures 3A and 4A). In three of eight pairs, the BC axon formed two or three putative inhibitory synaptic contacts with proximal portions of apical dendrites of the GC (Figures 3A and 3C). This indicates that reciprocal excitatory–inhibitory GC–BC connections occurred abundantly.

Submillisecond Postsynaptic Conductance Change

The location of the synaptic contacts of the GC–BC synapse, which were established close to the soma of the BC, allowed us to measure the postsynaptic conductance changes as EPSCs in the voltage-clamp configuration. A representative voltage-clamp experiment is illustrated in Figure 5A. In this pair, the synaptic latency, measured from the point of maximal slope in the rise of the presynaptic action potential to the beginning of the average EPSC, was 800 μs , consistent with the monosynaptic nature of transmission. The 20%–80% rise time of the average EPSC was 260 μs , and the decay was monoexponential, with a time constant of 580 μs . In nine pairs, the mean latency of the average EPSC was 892 ± 74 μs , and the 20%–80% rise time and the decay time constant of the average EPSC were 249 ± 15 μs and 772 ± 91 μs , respectively (Table 1). The kinetics of individual EPSCs were even faster than those of the average EPSC; in the pair shown, the fastest evoked events had 20%–80% rise times of ~ 80 μs and decay time constants of 200 μs (Figure 5A). Correlated morphological analysis of this pair revealed three putative synaptic contact sites (29, 41, and 84 μm from the soma), suggesting that the fastest events were generated at the proximal synaptic contact. The extremely fast time course of the excitatory postsynaptic conductance change at the GC–BC synapse is highlighted by comparison with the kinetics of the inhibitory BC–GC conductance change. A representative recording of BC–GC inhibitory postsynaptic currents (IPSCs) is shown in Figure 5B. Whereas the mean latency (864 ± 13 μs) and the 20%–80% rise time (193 ± 28 μs) of the IPSC generated at the BC–GC synapse were comparable to those of the EPSCs generated at the GC–BC synapse, the decay was markedly slower and biexponential (time constants, 0.9 ± 0.2 and 6.7 ± 1.3 ms, respectively; amplitude contribution of the fast component, $45\% \pm 10\%$; 3 pairs).

Time Course of Transmitter Release and Kinetics of Quantal EPSC Components

We then examined the contribution of pre- and postsynaptic mechanisms to the fast time course of the average EPSC. If the postsynaptic conductance change consisted of independent quantal contributions, the average EPSC would be the convolution of the time course of transmitter release and the kinetics of the quantal EPSC components (Katz, 1969; Isaacson and Walmsley, 1995). This hypothesis was tested at the GC–BC synapse in conditions of normal and reduced release probability. In the experiment shown in Figure 6, the release probability was reduced by decreasing the extracellular $\text{Ca}^{2+}/\text{Mg}^{2+}$ concentration ratio from 2 to 0.5 (del Castillo and Katz, 1954). As this ratio was reduced, the mean amplitude of the evoked EPSCs decreased from 326 pA (Figures 6A and 6B) to 142 pA (Figures 6C and 6D), and the number of failures increased accordingly (from 15% to 44%, in this pair; Figure 6C). This suggests that quantal EPSCs can be distinguished in these recording conditions, as proposed for the neuromuscular junction (del Castillo and Katz, 1954) and the calyx synapse in the brainstem (Isaacson and Walmsley, 1995).

To evaluate the time course of glutamate release at the GC–BC synapse, histograms of first quantal latencies were converted into release probability distributions (Barrett and Stevens, 1972; see Experimental Procedures and Figures 6E and 6F). In conditions of low release probability, which imply the highest accuracy of the first latency approach, the release probability distribution was very narrow, and decayed with a time constant of 298 ± 15 μs (4 pairs; Table 1).

To determine the decay time course of the quantal EPSCs, individual events recorded in conditions of low release probability (Figure 6C) were aligned by their rising phase and averaged. The mean decay time constant of the quantal EPSCs was 367 ± 29 μs (4 pairs; Table 1). Convolution of the release probability function with the quantal EPSC generated a simulated EPSC that closely matched the recorded average EPSC, independent of whether the release probability was normal or reduced (Figure 6F). The nonlinear correlation coefficient between measured and simulated EPSC, determined from the decay phase, was not significantly different from that between the measured EPSC and a directly fitted exponential function ($r = 0.993$ and 0.995 , respectively). These results indicate that the duration of the release period and the kinetics of the quantal EPSC are the main determinants in shaping the average postsynaptic conductance change, and that the impact of multivesicular release or cross-talk (e.g., Trussell et al., 1993) on the time course is minimal at this synapse.

Determinants Shaping the Time Course of the Quantal EPSC

To determine the contribution of gating of AMPARs to the rapid decay of the quantal EPSCs at the GC–BC synapse, we compared the kinetics of quantal EPSCs to those of AMPAR-mediated currents evoked by glutamate pulses in outside-out membrane patches isolated from BC somata.

At 22°C, the deactivation time constant was 1.3 ± 0.1 ms, whereas the desensitization time constant was $4.5 \pm$

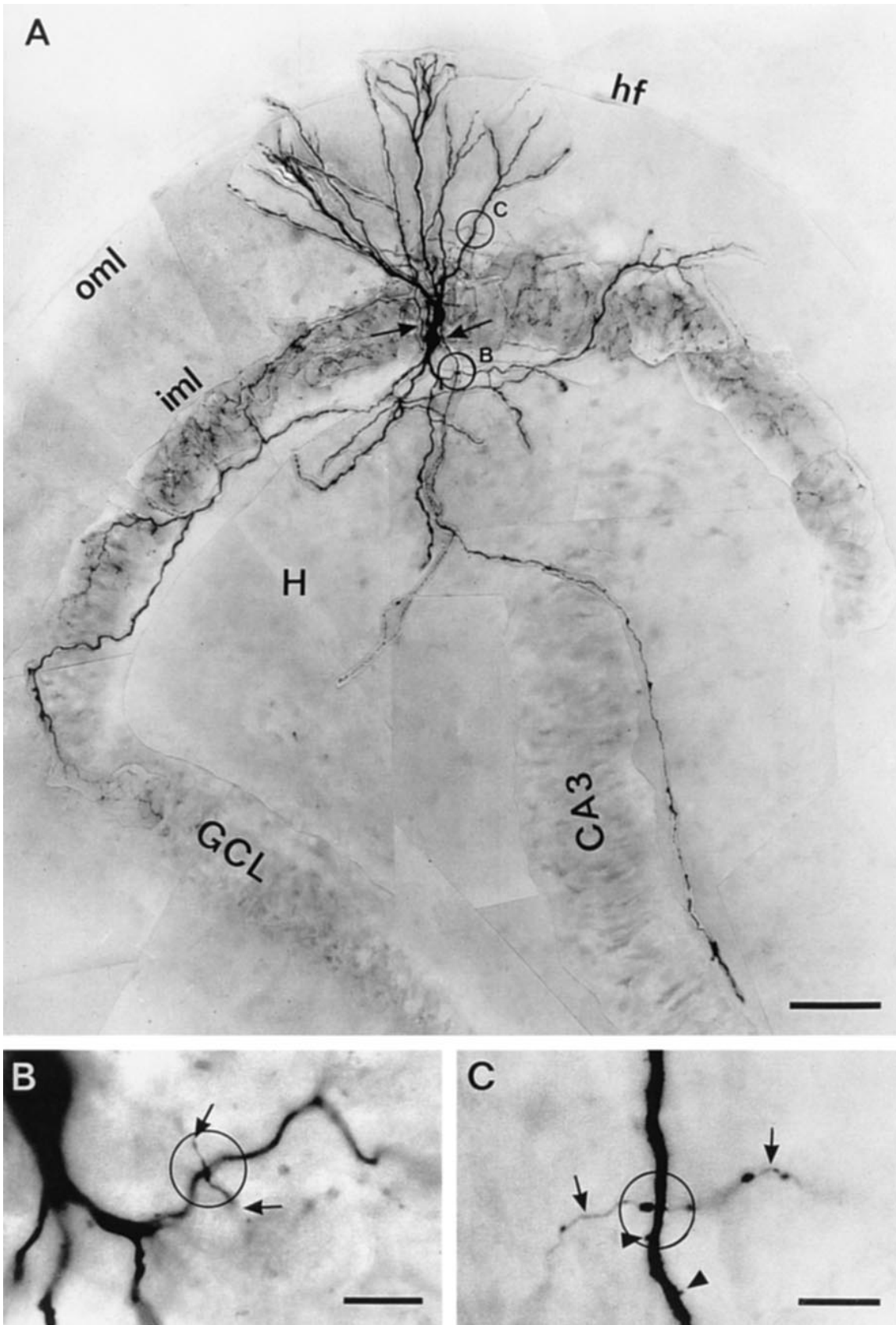


Figure 3. Light Microscopic Image of a Reciprocally Coupled, Biocytin-Filled GC-BC Pair

(A) Low power photomontage of a synaptically coupled GC-BC pair. Note the extensive arborization of the BC axon that spans almost the entire granule cell layer and the typical course of the GC mossy fiber axon that, after passing through the hilar region, runs parallel to the CA3 pyramidal cell layer. The origins of the main axons of the two neurons are marked by arrows. The open circles indicate putative synaptic contacts which are shown in (B) and (C) at higher magnification. Scale bar, 100 μ m. CA3 refers to the CA3 pyramidal cell layer; GCL to the granule cell layer; H to the hilar region; hf to the hippocampal fissure; iml to the inner molecular layer; and oml to the outer molecular layer.

0.9 ms (Figure 7A; 18 patches; 1 and 100 ms pulses of 1 mM glutamate, respectively). As the glutamate concentration was increased from 0.1 to 10 mM, the desensitization time constant decreased and reached an asymptotic value of 3.2 ms at the high concentration limit (Figure 7B). At the same recording temperature, the decay time constant of the quantal EPSCs was 1.3 ± 0.1 ms (2 pairs; Figure 7C). These results indicate that at 22°C the decay time constant of the quantal EPSCs is similar to the deactivation time constant, but markedly faster than the asymptotic value of the desensitization time constant (Figure 7D).

At 34°C, AMPAR deactivation kinetics could not be determined, due to limitations of the fast application technique. The asymptotic value of the desensitization time constant, however, was 1.8 ± 0.2 ms (4 patches), significantly longer than the decay time constant of both the quantal EPSC and the average EPSC ($P < 0.05$). Assuming that the functional properties of postsynaptic AMPARs are identical to those in somatic patches, these results indicate that the decay of the quantal EPSC is determined by AMPAR deactivation rather than desensitization, and imply that the glutamate pulse in the synaptic cleft at GC–BC synaptic contacts is extremely brief.

Time Course of the Postsynaptic Conductance Change Determines Shape of Single EPSPs and Temporal Summation of Multiple EPSPs

To address quantitatively how the time course of the postsynaptic conductance change at the GC–BC synapse influences the shape of single EPSPs and the temporal summation of multiple EPSPs, we performed simulations using a detailed passive cable model based on the morphology of a postsynaptic BC (Figure 8A). In the pair selected for this simulation, the experimentally determined mean half duration of the evoked EPSPs and the mean decay time constant of the evoked EPSCs were 3.2 ms and 306 μ s, respectively; the fastest EPSCs had a decay time constant of ~ 200 μ s (Figure 5A).

When a rapid conductance change (200 μ s decay time constant) was simulated at the sites of synaptic location, the kinetics of both the dendritic and the somatic EPSP were very rapid. The half duration of the simulated somatic EPSP for a rapid conductance change at site (a) was 3.1 ms (Figure 8B, traces labeled “1”), whereas that for simultaneous conductance changes at sites (a), (b), and (c) was 3.4 ms (not illustrated). When a slow conductance change (1.2 ms decay time constant) was simulated, the time courses of both the dendritic and the somatic EPSPs were markedly slower. The half duration of the simulated somatic EPSP for a slow conductance change at site (a) was 7.1 ms (Figure 8B, traces labeled “2”), whereas that for simultaneous conductance changes at sites (a), (b), and (c) was 7.2 ms (not illustrated). These results indicate a direct relation between the time course of the postsynaptic conductance

change and the shape of both the dendritic and the somatic EPSPs. While the shaping effect of the postsynaptic conductance change was stronger for the dendritic than for the somatic EPSP, the effect on the somatic EPSP may be functionally more important in determining the input–output relation of the BC.

To quantitate the relation between the time course of the postsynaptic conductance change and the temporal summation of multiple EPSPs, synaptic conductance changes separated by intervals of variable duration were simulated at the putative synaptic contact sites (a) and (b) (Figures 8C and 8D). The maximal amplitude of the summated EPSP was normalized and plotted against the time interval between the postsynaptic conductance changes in Figure 8D. When the conductance change with rapid time course was simulated, the window for temporal summation was very narrow (Figure 8D, closed circles; half width, 4.7 ms). When the conductance change with slower kinetics was simulated, the window for temporal summation was much wider (Figure 8D, open circles; half width, 9.7 ms). These results indicate that the time course of the postsynaptic conductance change sets the window for temporal summation of EPSPs.

Discussion

Combining whole-cell patch-clamp recording from pairs of synaptically coupled neurons with morphological analysis, we show that a submillisecond AMPAR-mediated conductance change underlies synaptic transmission at a hippocampal PN–IN synapse. The results suggest that the conductance change is shaped mainly by the time course of glutamate release from the presynaptic boutons and the deactivation of the postsynaptic AMPARs. For the given passive membrane properties of the IN, the specific functional and morphological characteristics of PN–IN synapses determine the shape and the somatodendritic integration of EPSPs. This may allow INs to operate as coincidence detectors.

Pre- and Postsynaptic Factors Determine the Submillisecond Postsynaptic Conductance Change

Both the asynchrony in the timing of exocytosis at a single release site from trial to trial and the number and spatial distribution of release sites of the entire synapse contribute to the duration of the release period. The timing of the glutamate release at the GC–BC synapse was highly precise, despite its distributed morphological nature (see below). The release probability distribution decayed with a mean time constant of 298 μ s, comparable to that of the calyx synapse in the cochlear nucleus (157 μ s; Isaacson and Walmsley, 1995; 30°C) or that of the mammalian neuromuscular junction (~ 200 μ s; Datyner and Gage, 1980; $>30^\circ\text{C}$). In contrast, autapses

(B) Putative excitatory synaptic contact (open circle) established by an en passant GC axonal collateral (marked by arrows) on a secondary basal dendrite of the BC. Scale bar, 25 μ m.

(C) Putative inhibitory synaptic contact (open circle) established by an en passant BC axonal collateral (marked by arrows) on a tertiary apical dendrite of the GC. Dendritic spines of the GC are marked by arrowheads. Scale bar, 25 μ m. The image shows the same GC–BC pair as Figure 4A.

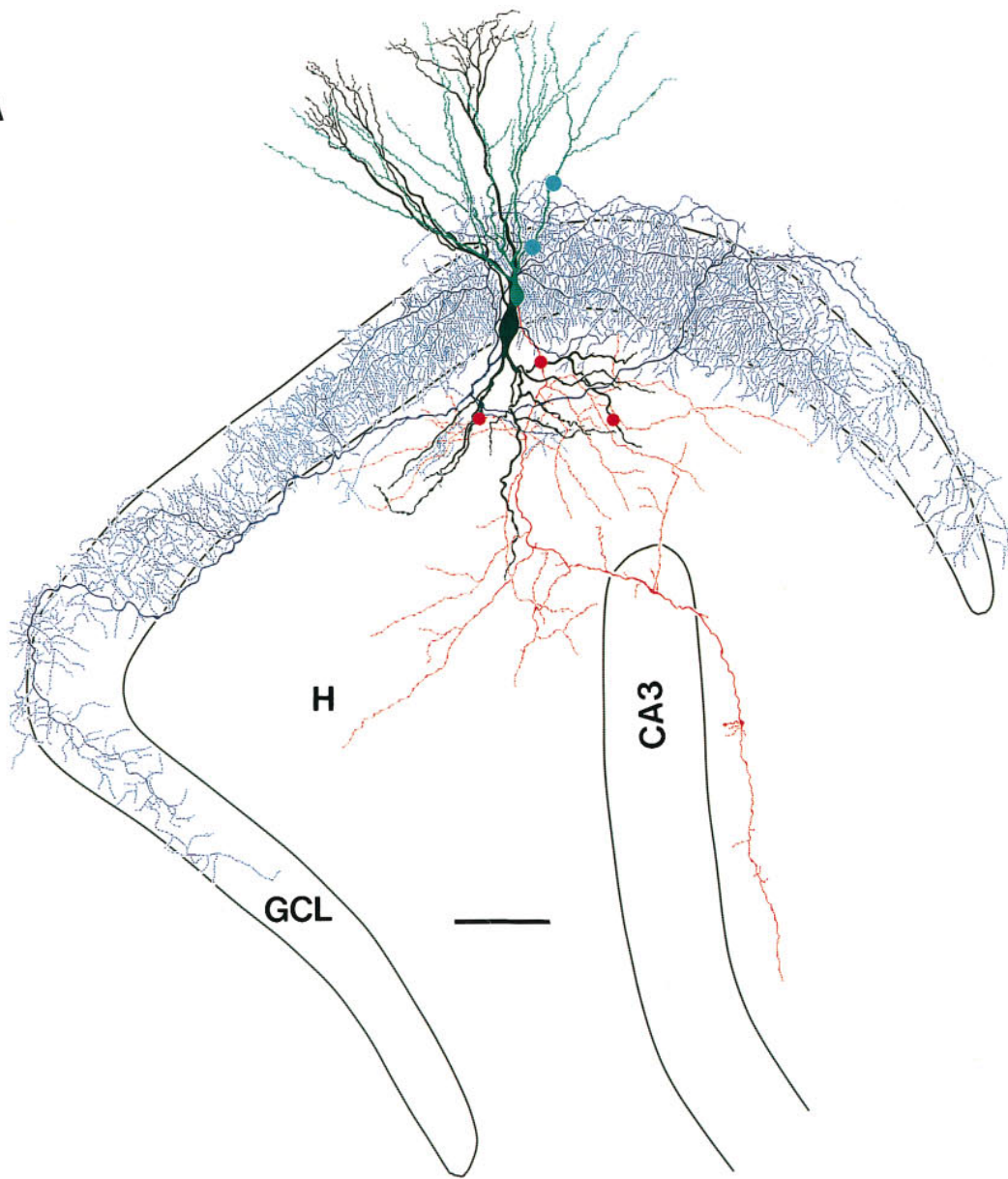
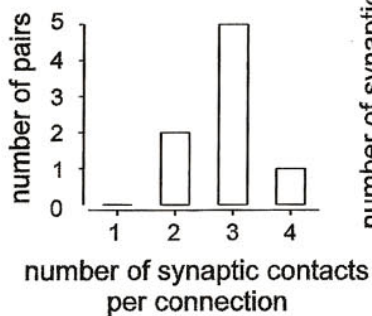
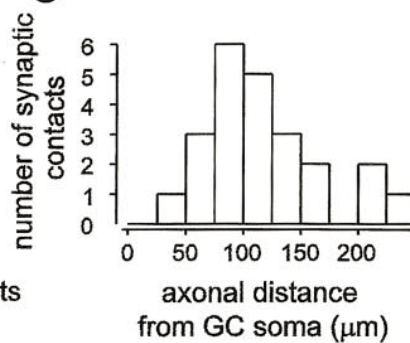
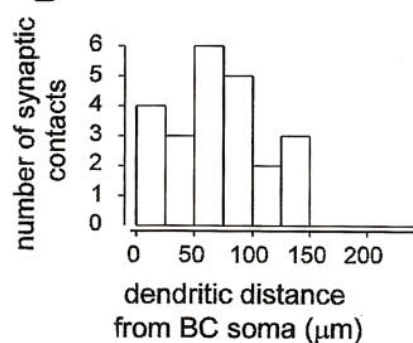
A**B****C****D**

Figure 4. Camera Lucida Reconstruction of a GC-BC Pair and Quantitative Analysis of the Number and Location of Putative Excitatory Synaptic Contacts

(A) A camera lucida reconstruction of the GC-BC pair shown in Figure 3. Green indicates the soma and dendrites of the GC. Red indicates the axonal arborization of the GC. Black indicates the soma and dendrites of the BC. Blue indicates the axonal arborization of the BC. Light microscopic analysis revealed three putative excitatory synaptic contacts (red circles) established by the GC axonal collaterals within the hilar region on different basal dendrites of the BC. In addition, two putative inhibitory synaptic contacts (blue circles) formed by different BC axonal collaterals on different apical dendrites of the GC were identified. Scale bar, 100 μm . For abbreviations, see Figure 3.

(B) A histogram of the number of putative excitatory synaptic contacts per GC-BC pair.

formed by cultured hippocampal PNs showed a longer release period, decaying with a time constant of 3.9 ms (Diamond and Jahr, 1995; 22°C). Assuming that the temperature dependence of the release process is the same for all synapses ($Q_{10} \approx 3$; Datyner and Gage, 1980; Isaacson and Walmsley, 1995), this may indicate that synchrony of release at the GC–BC synapse is higher than that at excitatory synapses between PNs.

The kinetics of evoked quantal EPSCs generated at the GC–BC synapse and recorded with a somatic patch pipette were very fast. Quantal EPSCs decayed with a mean time constant of 367 μ s. Hence, the kinetics of quantal EPSCs at the GC–BC synapse are comparable to those of calyx synapses on auditory relay neurons (τ_{decay} of miniature EPSCs, 180 μ s; 29°C–32°C; Zhang and Trussell, 1994a). In contrast, quantal EPSCs in PNs of the hippocampus decay much more slowly (τ_{decay} , 2.3 ms; 34°C; Tong and Jahr, 1994b). Hence, both the time course of transmitter release and the kinetics of the quantal postsynaptic conductance change at the GC–BC synapse are comparable to those of calyx synapses on auditory relay neurons, but appear to be markedly faster than those at synapses between PNs of the hippocampus.

The comparison of the time course of the quantal EPSC with the deactivation and desensitization time constant of AMPARs expressed in the BC (Koh et al., 1995) indicates that the decay of the quantal EPSC is determined by AMPAR deactivation at 22°C and 34°C. This implies that glutamate is cleared from the synaptic cleft of GC–BC synapses very rapidly. An upper limit of the duration of the glutamate pulse in the synaptic cleft is given by the sum of the rise and decay time of the quantal conductance change ($\sim 500 \mu$ s).

Convolution of the release probability distribution with the time course of the quantal EPSC gave a simulated EPSC that was indistinguishable from the average evoked EPSC, at both normal and reduced release probability. This may indicate that the quantal EPSCs superimpose independently, and that the contribution of cross-talk or multi-vesicular release to the time course of the average evoked EPSC at the GC–BC synapse is minimal (Trussell et al., 1993; Tong and Jahr, 1994a; Mennerick and Zorumski, 1995).

Target Cell-Specific Regulation of the EPSC Time Course by Differential Expression of AMPAR Subunits

Postsynaptic AMPARs at excitatory synapses are thought to be heteromeric channels assembled from four types of subunits (GluR1 to 4 or GluR-A to -D), each existing in two alternatively spliced versions (flip and flop; reviewed by Hollmann and Heinemann, 1994). Previous studies indicated that PNs and INs of the hippocampus differ in their AMPAR subunit mRNA content. While AMPARs of PNs are mainly assembled from GluR-A and -B subunits in the flip form, AMPARs of INs are dominated by GluR-A subunits but also contain

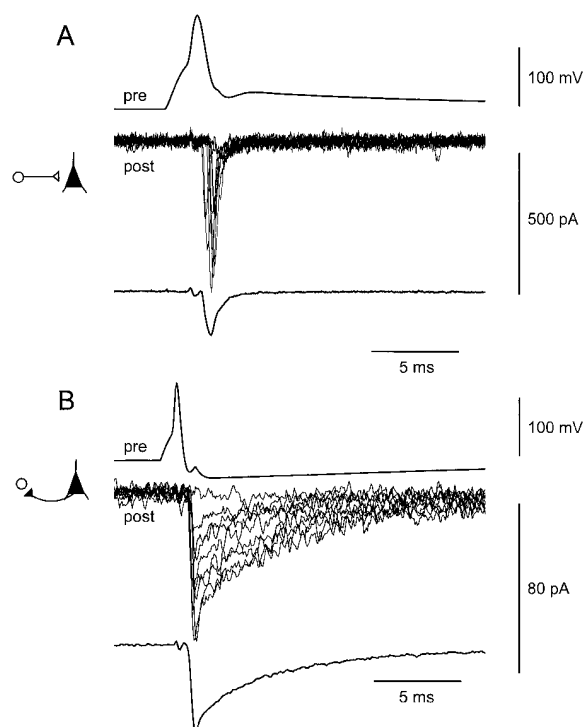


Figure 5. Conductance Changes Underlying Excitation and Inhibition in the GC–BC Circuitry

(A) Unitary EPSCs recorded in the BC at 34°C. Top trace shows the action potential in the presynaptic GC. The middle traces show the individual evoked EPSCs in the postsynaptic BC. The bottom trace shows the average EPSC of 250 individual traces. The latency of the average EPSC, measured from the maximum of the first derivative of the GC action potential to the beginning of the BC EPSC, was 800 μ s. The decay of the average EPSC was well fit by a single exponential (time constant, 580 μ s).

(B) Unitary IPSCs recorded in the GC. The top trace shows the action potential in the presynaptic BC. The middle traces show the individual evoked IPSCs in the postsynaptic GC. The bottom trace shows the average IPSC of 110 traces. The latency of the average BC–GC IPSC was 820 μ s. The decay of the average IPSC was biexponential (time constants, 1.1 ms and 7.2 ms; amplitude contribution of the fast component, 34%).

The data in (A) and (B) are from different pairs; the holding potential was -70 mV, in both cases. The pipette solutions for the postsynaptic neuron were K-gluconate intracellular solution (A) and KCl intracellular solution (B).

GluR-B to -D subunits in the flop form (Geiger et al., 1995). AMPARs expressed in the two types of neurons also differ markedly in functional properties that are relevant for the shaping of the EPSC decay; AMPARs expressed in INs show a 2-fold faster deactivation, a 3-fold faster desensitization, and a 2-fold higher value of the half-maximal activating glutamate concentration than those in PNs (Jonas and Sakmann, 1992; Koh et al., 1995). Low affinity and fast deactivation act cooperatively in speeding up the EPSC time course; for a given peak concentration and decay time course of a synaptic

(C) A histogram of the axonal distance from the GC soma to the putative synaptic contact.

(D) A histogram of the dendritic distance from the BC soma to the putative synaptic contact. The data in (B–D) are from 23 putative excitatory synaptic contacts of eight fully reconstructed GC–BC pairs.

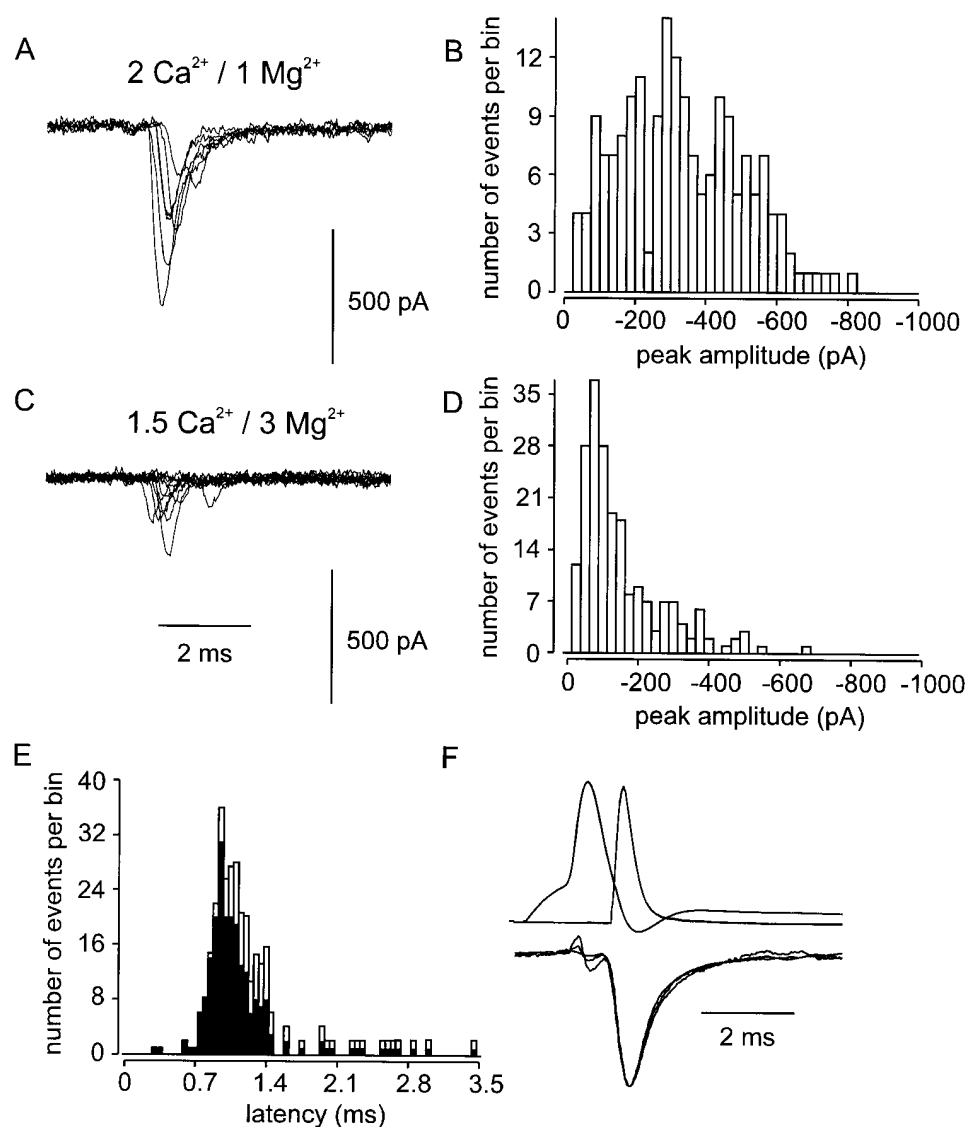


Figure 6. Time Course of Quantal Transmitter Release at the GC-BC Synapse

(A and B) Unitary EPSCs recorded in the presence of 2 mM external Ca^{2+} and 1 mM external Mg^{2+} . The individual traces are shown in (A), and a peak amplitude histogram is illustrated in (B). Number of events, 184; number of failures, 33.

(C and D) Quantal EPSCs recorded in the presence of 1.5 mM Ca^{2+} and 3 mM Mg^{2+} . The individual traces are shown in (C), and the peak amplitude histogram is depicted in (D). Number of events, 218; number of failures, 171. The change in the shape of the amplitude distribution was consistent with synaptic transmission mediated by a small number of release sites.

(E) A first latency histogram (filled bars) and release probability distribution (open bars) of EPSCs obtained by the correction method of Barrett and Stevens (1972; 1.5 mM Ca^{2+} and 3 mM Mg^{2+}). Fitting the decay of the release probability distribution with a single exponential gives a time constant of 314 μs .

(F) The upper trace shows the action potential in the presynaptic GC and the release probability function superimposed. The release histogram (in E) was fitted with a skewed gamma-type function: $f(t) = A(t - \delta t)^a \exp[-(t - \delta t)/\tau_1] + B \exp[-(t - \delta t)/\tau_2]$ for $t > \delta t$; $f(t) = 0$ for $t \leq \delta t$, with $\tau_1 = 108 \mu\text{s}$, $\tau_2 = 985 \mu\text{s}$, $a = 2.3$, $A = 6.9 \cdot 10^3$, and $B = 3.5$. The lower trace shows the simulated EPSC, the average EPSC in 2 mM Ca^{2+} and 1 mM Mg^{2+} , and the average EPSC in 1.5 mM Ca^{2+} and 3 mM Mg^{2+} , normalized and superimposed. The simulated EPSC was obtained by convolution of the release probability function and the average of 50 quantal EPSCs aligned by their rising phase. The holding potential was -70 mV . The pipette solution for the BC was K-gluconate intracellular solution.

All data were obtained from the same GC-BC pair.

glutamate pulse, the low affinity for glutamate favors channel closure by deactivation. Studies on recombinant and native AMPARs indicated that slow gating kinetics are conferred by GluR-B_{flip} subunits (Burnashev, 1993; Geiger et al., 1995), whereas fast gating kinetics

are due to the presence of GluR-D subunits in heteromeric combinations (Mosbacher et al., 1994; Geiger et al., 1995). Given that the decay of the quantal EPSC is largely shaped by AMPAR deactivation, this suggests that differential expression of AMPAR subunit genes in

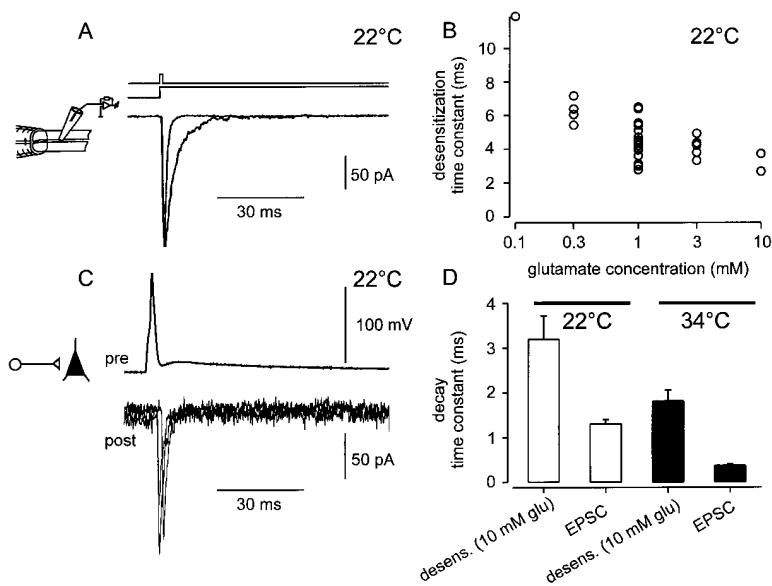


Figure 7. AMPAR Deactivation Shapes the Decay of Quantal EPSCs

(A) Traces of current activated by a 1 and a 100 ms pulse of 1 mM glutamate in an outside-out patch isolated from the soma of a BC. The recording temperature was 22°C; the holding potential was -60 mV.

(B) Weak concentration dependence of the desensitization time constant of BC AMPARs. The data are from 22 outside-out patches at 22°C. Note that the desensitization time constant approaches an asymptotic value at high glutamate concentrations.

(C) Quantal EPSCs at the GC–BC synapse recorded at 22°C, plotted at the same time scale as the traces in (A). The percentage of failures was 82.5%; three traces are shown superimposed. The action potential evoked in the presynaptic GC is shown on top. Note that the decay of the EPSC is almost identical to the deactivation time course of the glutamate-activated current (1 ms pulse).

(D) A comparison of the asymptotic value of the desensitization time constant of BC AMPARs with the decay time constant of the EPSC at 22°C and 34°C. Note that the decay time constant of the EPSC is markedly faster than the asymptotic value of the desensitization time constant, irrespective of the recording temperature.

the postsynaptic target cells controls the time course of the EPSC in PNs and INs of the hippocampal circuitry.

Impact of Morphological Properties on Fast Signaling at the GC–BC Synapse

GC–BC synapses are characterized by three main morphological properties: the distributed nature of the synapse (2–4 putative synaptic contacts), the small diameter (~ 1 μm) of the presynaptic boutons, and the absence of spines on the postsynaptic BC dendrites. The presence of multiple synaptic contacts, which is consistent with the observation that the evoked EPSC is made up from independent quantal contributions (Figure 6), may enhance the efficacy of synaptic transmission. Consistent with this notion, EPSPs generated at this synapse have a larger amplitude (mean, 2.1 mV; Table 1) than those at a PN–IN synapse in the CA3 region of the hippocampus, mediated by a single release site (0.65 mV; Gulyás et al., 1993).

The separation between individual synaptic contacts of the same connection, the limited size of the presynaptic elements, and the smooth surface of the postsynaptic dendrites may facilitate transmitter clearance from the synaptic cleft by diffusion (Eccles and Jaeger, 1958; Barbour et al., 1994; Wahl et al., 1996) and could minimize the effects of cross-talk (Trussell et al., 1993). This suggests that the GC–BC synaptic contacts act as independent units that are optimized for fast signaling.

A potential disadvantage of the distributed arrangement is that the action potential of the presynaptic GC reaches different boutons at slightly different times. The axonal pathways leading to the boutons of one connection varied in length by 39 μm on average (Table 1). Assuming a conduction velocity of 0.3 m s^{-1} for the

action potential in unmyelinated axons of the hippocampus (Andersen et al., 1978), the axonal conduction time may differ by 100 μs between different synaptic contacts. This could imply that the timing of release at individual GC–BC synaptic contacts is even more precise than the overall time course of the release period.

Somatodendritic Integration of EPSPs and Input–Output Relation of GABAergic INs

Precise timing of release, fast deactivation of the postsynaptic AMPARs, and specific morphological properties of the GC–BC synapse contribute to the generation of EPSPs with rapid time course, in conjunction with passive membrane properties of the postsynaptic neuron. The dendritic EPSP is very fast, shaped largely by the postsynaptic conductance change, as suggested previously for thin dendrites (Softky, 1994). The fast shape is remarkably conserved as the EPSP spreads from the dendrite to the soma and the axon initial segment, the putative site of action potential initiation (Stuart et al., 1997). This is due to the strategic location of the synaptic contacts electrotonically close to the soma of the postsynaptic BC. As a final consequence, the time course of the somatic EPSPs generated by the GC–BC synapse (half duration, 3.7 ms) is much faster than that of EPSPs at synapses between PNs in the hippocampus (half duration, 27 ms; Miles and Wong, 1986; 37°C) and neocortex (τ_{decay} , 40 ms; Markram et al., 1997; 32°C–34°C).

The half duration of the EPSP generated at the GC–BC synapse is significantly faster than that of PN–IN EPSPs in the CA3 region of the hippocampus (half duration, 9.8 ms; Miles, 1990) but is comparable to that of PN–IN EPSPs in the neocortex (4.8 ms; Thomson et al., 1993).

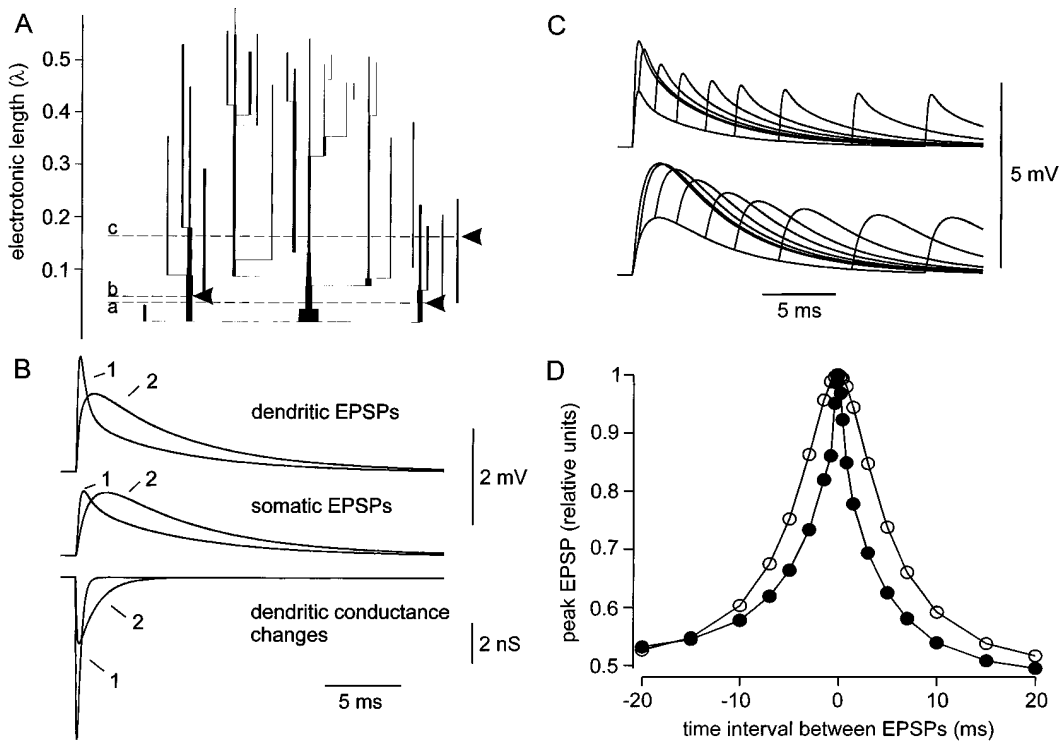


Figure 8. Time Course of the Postsynaptic Conductance Change Determines the Shape and Somatodendritic Integration of EPSPs

(A) An electrotonic dendrogram of a BC dendritic tree. Apical dendrites are represented in the center; basal dendrites are shown laterally in the dendrogram. The axonal arborization is not drawn. The locations of the three putative synaptic contacts formed by the axon of the presynaptic GC are indicated by horizontal dashed lines and arrowheads. The electrotonic length of each segment was calculated from the physical length (l) and diameter (d) as $L = l/\lambda$, where the space constant λ was $\sqrt{(R_m d / 4 R)}$. The BC depicted here is the postsynaptic target cell of the pair in Figure 5A. The physical and electrotonic distances of the three putative synaptic contacts from the soma were 29, 41, and 84 μm and 0.04, 0.05, and 0.16 λ , respectively.

(B) The upper and middle traces show simulations of dendritic and somatic EPSPs in the current-clamp mode. The lower traces show underlying postsynaptic conductance changes. The time course of the postsynaptic conductance change was represented by the function $-\exp(-t/\tau_{\text{rise}}) + \exp(-t/\tau_{\text{decay}})$ and was simulated at putative synaptic contact site (a). Traces denoted as 1 were obtained by simulation of a rapid postsynaptic conductance change ($\tau_{\text{rise}} = 80 \mu\text{s}$; $\tau_{\text{decay}} = 200 \mu\text{s}$; peak conductance, 8 nS). Traces denoted as 2 were obtained by simulation of a slow postsynaptic conductance change ($\tau_{\text{rise}} = 80 \mu\text{s}$; $\tau_{\text{decay}} = 1.2 \text{ms}$; peak conductance, 3.2 nS).

(C and D) A temporal summation of multiple EPSPs. Postsynaptic conductance changes separated by intervals of variable duration were simulated at the putative synaptic contact sites (a) and (b). (C) Simulated somatic EPSP traces for a fast (upper traces) and a slow (lower traces) postsynaptic conductance change are shown. (D) The amplitude of the summated somatic EPSP, normalized to the maximal amplitude, was plotted against the time interval between the simulated conductance changes for a fast (closed circles) and a slow (open circles) postsynaptic conductance change. The positive value of the time interval indicates that synaptic conductance change at contact (a) precedes that at contact (b).

The membrane properties of the postsynaptic INs cannot account for these differences, because the apparent membrane time constants of these neurons are similar (8.4 ms for BCs, this paper; 9.0 ms for CA3 INs, Miles, 1990; 11.9 ms for neocortical INs, McCormick et al., 1985). The differences in EPSP time course may be due to variation in the location of the synaptic contacts. We cannot exclude the possibility, however, that excitatory synapses on different types of GABAergic INs in the cortex differ in the synchrony of transmitter release or in the subunit composition of the postsynaptic AMPARs.

The different time courses of EPSPs in INs and PN suggest that the two types of neurons perform different computational tasks, and that INs operate as coincidence detectors (Softky, 1994), whereas PNs may behave as temporal integrators (Shadlen and Newsome, 1994). The rapid time course and the subthreshold amplitude of unitary EPSPs at the GC-BC synapse implies

that action potential initiation in the BC will require synchronous activity of an ensemble of GCs. On the basis of the average EPSP amplitude (0.7–3 mV), the resting membrane potential ($\sim -65 \text{mV}$), and the action potential initiation threshold ($\sim -50 \text{mV}$), we estimate that 5–20 GCs converging onto the BC have to fire in synchrony. This would correspond to 0.5%–2% of all the GCs innervating a BC (Patton and McNaughton, 1995). Alternatively, coactivation of mossy cells (Scharfman, 1995) or neurons of the entorhinal cortex (reviewed by Freund and Buzsáki, 1996) with a correspondingly smaller number of GCs will initiate action potentials in the postsynaptic BC. Hence, BC-mediated recurrent inhibition may be triggered by the synchronous activity of a small number of GCs (about 10), but will provide a synchronization signal to a large number of GCs (about 14,000; Patton and McNaughton, 1995; Cobb et al., 1995).

Submillisecond signaling at PN-IN synapses in the

hippocampus resembles that between neurons of the auditory system with respect to the very rapid time course of both EPSPs and EPSCs (Zhang and Trussell, 1994a, 1994b). While coincidence detection in auditory neurons permits sound localization on the basis of interaural time differences (Reyes et al., 1996), the functional significance of coincidence detection in INs for the operation of the hippocampal network is, at present, unclear. Fast excitation of INs may help to establish the long-range coherence of oscillatory activity in cortical PN–IN networks (Traub et al., 1996) and could thus provide the context for temporal encoding of information in spatially distributed PN ensembles (Buzsáki and Chrobak, 1995; Cobb et al., 1995; Jefferys et al., 1996).

Experimental Procedures

Patch-Clamp Recording

Transverse hippocampal slices (300 μm thickness) were cut from the brains of 15- to 23-day-old Wistar rats using a vibratome (DTK-1000, Dosaka). In the dentate gyrus, granule cells and basket cells were identified visually using infrared differential interference contrast videomicroscopy (Koh et al., 1995). To obtain simultaneous recordings from synaptically coupled GCs and BCs, a tight-seal ($>2\text{ G}\Omega$) whole-cell recording configuration was established in the visually identified BC. Patch pipettes of low resistance (0.7–2 M Ω), pulled from thick-walled borosilicate glass tubing (2 mm outer diameter, 0.5 mm wall thickness), were used. Only neurons showing resting potentials more negative than -60 mV , high-frequency trains of action potentials on sustained current injection, and fast spontaneous EPSCs (providing an indication for local synaptic connectivity) were selected for paired recordings. Individual GCs were approached with a second, smaller pipette (3–10 M Ω). K^+ -rich solution leaking from the pipette allowed us to identify GCs likely to be synaptically connected to the given BC by an increase in the EPSC frequency. A tight-seal whole-cell recording was obtained, and action potentials were evoked in the GC. The probability of excitatory synaptic coupling between the GC and the BC was up to 20%. Synaptically coupled GCs and BCs were typically separated from each other by $<50\text{ }\mu\text{m}$, and were located 30–50 μm below the surface of the slice.

Two independent Axopatch 200A amplifiers (Axon Instruments) were used for current- and voltage-clamp recording. The presynaptic neuron was held in the current-clamp mode and was stimulated at a rate of 0.25–1 s^{-1} . Action potentials were initiated by 2 or 3 ms current pulses. The postsynaptic cell was held either in the current- or in the voltage-clamp mode. In the voltage-clamp mode, series resistance (R_s) compensation was employed (nominally $\sim 95\%$, lag 35–100 μs ; R_s before compensation, 3.5–10 M Ω). The constancy of R_s during the experiment was assessed from the amplitude of the capacitive current in response to a 2 mV pulse. EPSPs and EPSCs were filtered at 5 or 10 kHz using the 4-pole low-pass Bessel filter of the amplifier, and were digitized at 10–40 kHz using a 1401 plus laboratory interface (equipped with 12- or 16-bit DA/AD converters; Cambridge Electronic Design) interfaced to a 486-PC. The EPC software package (version 6.0) from CED was used for stimulus generation and data acquisition. The peak amplitude of the evoked EPSP or EPSC was stable for $\sim 10\text{ min}$ but decreased at later times in some experiments. Data acquisition was restricted to the stable period. The temperature in the recording chamber was $34^\circ\text{C} \pm 2^\circ\text{C}$ throughout the experiment, unless otherwise indicated. Recordings were made from 55 synaptically coupled pairs of neurons.

Fast application experiments on outside-out patches isolated from BC somata were performed as described (Colquhoun et al., 1992). The 20%–80% exchange time of the application system, measured from the open tip response, was $<100\text{ }\mu\text{s}$, and the resistance of the patch pipettes used was 5–10 M Ω . Glutamate-activated currents were recorded either at 22°C or at 34°C ; in the latter case, the bath temperature was 34°C , and the fast application system was also maintained at 34°C using heat radiators (room temperature: 30°C).

Data Analysis

Evoked EPSPs and EPSCs were analyzed using programs written in Pascal by P. J., similar to those described previously (Jonas et al., 1993). The synaptic latency was determined as the time interval between the maximum of the first derivative of the presynaptic action potential and the beginning of the first EPSC following the action potential (e.g., Borst et al., 1995). The decay phase of the EPSPs/EPSCs was fitted with either one or two exponentials using a least-squares algorithm. Presynaptic voltage and postsynaptic current traces were shifted, with respect to each other, by up to 450 μs to correct for differences in the filter frequency and the response time of the current- and voltage-clamp configuration. Individual traces shown in the figures were passed through an additional digital filter (10 kHz).

Average EPSCs were generated from 24–300 individual traces aligned by the rising phase of the presynaptic action potentials. The time course of quantal release was determined from the first latency histogram, using the method of Barrett and Stevens (1972). The time course of the quantal EPSC was determined in conditions of reduced release probability (Figure 6); single quantal events were aligned by their rising phase and averaged. Finally, the release probability distribution was reconvolved with the average quantal EPSCs by multiplying the respective discrete Fourier transforms, using Mathematica 2.2 (Wolfram Research). All values are given as mean \pm SEM. Error bars also indicate SEM. Significance of differences was assessed by two-tailed Wilcoxon–Mann–Whitney test at the significance level (P) indicated.

Morphological Reconstruction and Analysis

For light microscopy, the pre- and postsynaptic neurons were filled with biocytin (0.5%) in K-gluconate solution during recording. After withdrawal of the pipettes, slices were kept for a further 30 min in the recording chamber to allow for sufficient axonal transport of the tracer. Slices were then fixed in 100 mM phosphate buffer (PB, pH 7.4) containing 1% paraformaldehyde and 2.5% glutaraldehyde (12 hr, 4°C). Subsequently, slices were processed for light microscopy as previously described (Kawaguchi and Kubota, 1996; Markram et al., 1997).

The morphology of the pre- and postsynaptic neurons of the synaptically coupled pairs was reconstructed with the aid of a camera lucida at a final magnification of $480\times$. In all pairs investigated, the axonal arborization of the postsynaptic BC was mainly confined ($>95\%$) to the granule cell layer, confirming the identification of the neuron as a BC (Buhl et al., 1995). The axonal arborization of the presynaptic GCs was similar to that described for adult granule cells (Amaral and Dent, 1981).

The camera lucida drawings formed the basis for subsequent quantitative analysis. The following parameters were estimated: 1) the number of putative synaptic contacts; 2) the axonal distance from the GC soma to the putative synaptic contact; 3) the dendritic distance from the BC soma to the putative synaptic contact; 4) the diameter of boutons of the GC axon in the hilar region; and 5) the diameter of mossy fiber boutons in the CA3 region.

Axons and dendrites of the pre- and postsynaptic neurons were examined using a $100\times$ oil immersion objective. Putative synaptic contacts were identified as the close appositions of a bouton and a dendrite in the same focal plane (Markram et al., 1997).

Solutions

For the synaptic experiments, the physiological extracellular solution contained 125 mM NaCl, 25 mM NaHCO_3 , 25 mM glucose, 2.5 mM KCl, 1.25 mM NaH_2PO_4 , 2 mM CaCl_2 , and 1 mM MgCl_2 . When the contribution of NMDARs to the EPSP/EPSC was studied, 10 μM glycine was added to the extracellular solution. The intracellular solution contained either 145 mM KCl, 0.1 mM EGTA, 2 mM MgCl_2 , 2 mM Na_2ATP , and 10 mM HEPES (KCl intracellular solution) or 135 mM K-gluconate, 20 mM KCl, 0.1 mM EGTA, 2 mM MgCl_2 , 2 mM Na_2ATP , and 10 mM HEPES (K-gluconate intracellular solution); the pH was adjusted to 7.3 with KOH. Dual component EPSCs at -70 and $+50\text{ mV}$ were recorded using Cs-gluconate intracellular solution containing 110 mM Cs-gluconate, 20 mM CsCl, 10 mM EGTA, 2 mM MgCl_2 , 2 mM Na_2ATP , 10 mM HEPES, and 8 mM tetraethylammonium-Cl; the pH was adjusted to 7.3 with CsOH. For the fast application experiments, the external solution used for perfusing the application pipette contained 135 mM NaCl, 5.4 mM KCl, 1.8 mM CaCl_2 ,

1 mM MgCl₂, and 5 mM HEPES; the pH was adjusted to 7.2 with NaOH. The internal solution for filling the patch pipette contained 140 mM KCl, 10 mM EGTA, 2 mM MgCl₂, 2 mM Na₂ATP, and 10 mM HEPES; the pH was adjusted to 7.3 with KOH. CNQX and D-AP5 were from Tocris; all other chemicals were from Merck or Sigma.

Simulations

Detailed passive cable modeling (Major et al., 1994) was performed using one of the reconstructed GC-BC pairs. The diameters and three-dimensional coordinates of all dendritic segments and the main axon, including the first order collaterals of the BC, were determined using NeuroLucida (MicroBrightField). Due to the absence of spines on BC dendrites, no correction of the surface area was necessary. In addition, no correction was made for tissue shrinkage due to fixation. The axonal arborization was approximated by connecting 150 cylinders (diameter, 0.9 μm; length, 42 μm) to the main axonal collaterals.

EPSPs and EPSCs were simulated using NEURON (Hines, 1993), running on a Sparcstation 5 (Sun Microsystems). The electrical properties of the BC were assumed to be uniform. C_m was assumed to be 0.8 μF cm⁻². R_i was assumed to be 100 Ω cm; this value was chosen because, with the low-resistance recording pipettes used, the intracellular compartment is likely to be largely dialyzed by internal solution. R_m was assumed to be 10,000 Ω cm² (adjusted to match the input resistance of the BC measured at the soma). The resting potential was set to -70 mV. In voltage-clamp simulations, the residual uncompensated R_s was assumed to be 100 kΩ. The maximum segment length was 5.3 μm, and the time step in all simulations was 5 μs.

Acknowledgments

We thank Drs. J. Bischofberger, M. Häusser, and I. Vida for critically reading the manuscript; S. Nestel, B. Joch, M. Winter, B. Freudenberg, and K. Zipfel for excellent technical assistance; and B. Hillers for typing. Supported by the DFG (SFB 505/C5 to P. J. and Leibniz program to M. F.).

Received April 10, 1997; revised May 1, 1997.

References

Amaral, D.G., and Dent, J.A. (1981). Development of the mossy fibers of the dentate gyrus: I. A light and electron microscopic study of the mossy fibers and their expansions. *J. Comp. Neurol.* **195**, 51–86.

Andersen, P., Silfvenius, H., Sundberg, S.H., Sveen, O., and Wigström, H. (1978). Functional characteristics of unmyelinated fibres in the hippocampal cortex. *Brain Res.* **144**, 11–18.

Barbour, B., Keller, B.U., Llano, I., and Marty, A. (1994). Prolonged presence of glutamate during excitatory synaptic transmission to cerebellar Purkinje cells. *Neuron* **12**, 1331–1343.

Barrett, E.F., and Stevens, C.F. (1972). The kinetics of transmitter release at the frog neuromuscular junction. *J. Physiol.* **227**, 691–708.

Bekkers, J.M., and Stevens, C.F. (1989). NMDA and non-NMDA receptors are co-localized at individual excitatory synapses in cultured rat hippocampus. *Nature* **341**, 230–233.

Borst, J.G.G., Helmchen, F., and Sakmann, B. (1995). Pre- and post-synaptic whole-cell recordings in the medial nucleus of the trapezoid body of the rat. *J. Physiol.* **489**, 825–840.

Buhl, E.H., Cobb, S.R., Halasy, K., and Somogyi, P. (1995). Properties of unitary IPSPs evoked by anatomically identified basket cells in the rat hippocampus. *Eur. J. Neurosci.* **7**, 1989–2004.

Burnashev, N. (1993). Recombinant ionotropic glutamate receptors: functional distinctions imparted by different subunits. *Cell. Physiol. Biochem.* **3**, 318–331.

Buzsáki, G., and Chrobak, J.J. (1995). Temporal structure in spatially organized neuronal ensembles: a role for interneuronal networks. *Curr. Opin. Neurobiol.* **5**, 504–510.

Clements, J.D., Lester, R.A.J., Tong, G., Jahr, C.E., and Westbrook, G.L. (1992). The time course of glutamate in the synaptic cleft. *Science* **258**, 1498–1501.

Cobb, S.R., Buhl, E.H., Halasy, K., Paulsen, O., and Somogyi, P. (1995). Synchronization of neuronal activity in hippocampus by individual GABAergic interneurons. *Nature* **378**, 75–78.

Colquhoun, D., Jonas, P., and Sakmann, B. (1992). Action of brief pulses of glutamate on AMPA/kainate receptors in patches from different neurones of rat hippocampal slices. *J. Physiol.* **458**, 261–287.

Datnyer, N.B., and Gage, P.W. (1980). Phasic secretion of acetylcholine at a mammalian neuromuscular junction. *J. Physiol.* **303**, 299–314.

Debanne, D., Guérineau, N.C., Gähwiler, B.H., and Thompson, S.M. (1995). Physiology and pharmacology of unitary synaptic connections between pairs of cells in areas CA3 and CA1 of rat hippocampal slice cultures. *J. Neurophysiol.* **73**, 1282–1294.

del Castillo, J., and Katz, B. (1954). Quantal components of the end-plate potential. *J. Physiol.* **124**, 560–573.

Diamond, J.S., and Jahr, C.E. (1995). Asynchronous release of synaptic vesicles determines the time course of the AMPA receptor-mediated EPSC. *Neuron* **15**, 1097–1107.

Eccles, J.C., and Jaeger, J.C. (1958). The relationship between the mode of operation and the dimensions of the junctional regions at synapses and motor end-organs. *Proc. R. Soc. Lond. [Biol]* **148**, 38–56.

Freund, T.F., and Buzsáki, G. (1996). Interneurons of the hippocampus. *Hippocampus* **6**, 347–470.

Geiger, J.R.P., Melcher, T., Koh, D.-S., Sakmann, B., Seeburg, P.H., Jonas, P., and Monyer, H. (1995). Relative abundance of subunit mRNAs determines gating and Ca²⁺ permeability of AMPA receptors in principal neurons and interneurons in rat CNS. *Neuron* **15**, 193–204.

Gulyás, A.I., Miles, R., Sik, A., Tóth, K., Tamamaki, N., and Freund, T.F. (1993). Hippocampal pyramidal cells excite inhibitory neurons through a single release site. *Nature* **366**, 683–687.

Hestrin, S. (1993). Different glutamate receptor channels mediate fast excitatory synaptic currents in inhibitory and excitatory cortical neurons. *Neuron* **11**, 1083–1091.

Hines, M. (1993). NEURON—A program for simulation of nerve equations. In *Neural Systems: Analysis and Modeling*, F. Eeckman, ed. (Norwell, Massachusetts: Kluwer), pp. 127–136.

Hollmann, M., and Heinemann, S. (1994). Cloned glutamate receptors. *Annu. Rev. Neurosci.* **17**, 31–108.

Isaacson, J.S., and Walmsley, B. (1995). Counting quanta: direct measurements of transmitter release at a central synapse. *Neuron* **15**, 875–884.

Jack, J.J.B., and Redman, S.J. (1971). The propagation of transient potentials in some linear cable structures. *J. Physiol.* **215**, 283–320.

Jefferys, J.G.R., Traub, R.D., and Whittington, M.A. (1996). Neuronal networks for induced '40 Hz' rhythms. *Trends Neurosci.* **19**, 202–208.

Jonas, P., Major, G., and Sakmann, B. (1993). Quantal components of unitary EPSCs at the mossy fibre synapse on CA3 pyramidal cells of rat hippocampus. *J. Physiol.* **472**, 615–663.

Jonas, P., Racca, C., Sakmann, B., Seeburg, P.H., and Monyer, H. (1994). Differences in Ca²⁺ permeability of AMPA-type glutamate receptor channels in neocortical neurons caused by differential GluR-B subunit expression. *Neuron* **12**, 1281–1289.

Jonas, P., and Sakmann, B. (1992). Glutamate receptor channels in isolated patches from CA1 and CA3 pyramidal cells of rat hippocampal slices. *J. Physiol.* **455**, 143–171.

Katz, B. (1969). *The Release of Neural Transmitter Substances* (Liverpool: Liverpool University Press).

Kawaguchi, Y., and Kubota, Y. (1996). Physiological and morphological identification of somatostatin- or vasoactive intestinal polypeptide-containing cells among GABAergic cell subtypes in rat frontal cortex. *J. Neurosci.* **16**, 2701–2715.

Koh, D.-S., Geiger, J.R.P., Jonas, P., and Sakmann, B. (1995). Ca²⁺-permeable AMPA and NMDA receptor channels in basket cells of rat hippocampal dentate gyrus. *J. Physiol.* **485**, 383–402.

König, P., Engel, A.K., and Singer, W. (1996). Integrator or coincidence detector? The role of the cortical neuron revisited. *Trends Neurosci.* **19**, 130–137.

- Lacaille, J.-C., Mueller, A.L., Kunkel, D.D., and Schwartzkroin, P.A. (1987). Local circuit interactions between oriens/alveus interneurons and CA1 pyramidal cells in hippocampal slices: electrophysiology and morphology. *J. Neurosci.* *7*, 1979–1993.
- Lambolez, B., Ropert, N., Perrais, D., Rossier, J., and Hestrin, S. (1996). Correlation between kinetics and RNA splicing of α -amino-3-hydroxy-5-methylisoxazole-4-propionic acid receptors in neocortical neurons. *Proc. Natl. Acad. Sci. USA* *93*, 1797–1802.
- Major, G., Larkman, A.U., Jonas, P., Sakmann, B., and Jack, J.J.B. (1994). Detailed passive cable models of whole-cell recorded CA3 pyramidal neurons in rat hippocampal slices. *J. Neurosci.* *14*, 4613–4638.
- Markram, H., Lübke, J., Frotscher, M., Roth, A., and Sakmann, B. (1997). Physiology and anatomy of synaptic connections between thick tufted pyramidal neurones in the developing rat neocortex. *J. Physiol.* *500*, 409–440.
- McBain, C., and Dingledine, R. (1992). Dual-component miniature excitatory synaptic currents in rat hippocampal CA3 pyramidal neurons. *J. Neurophysiol.* *68*, 16–27.
- McCormick, D.A., Connors, B.W., Lighthall, J.W., and Prince, D.A. (1985). Comparative electrophysiology of pyramidal and sparsely spiny stellate neurons of the neocortex. *J. Neurophysiol.* *54*, 782–806.
- Mennerick, S., and Zorumski, C.F. (1995). Presynaptic influence on the time course of fast excitatory synaptic currents in cultured hippocampal cells. *J. Neurosci.* *15*, 3178–3192.
- Miles, R. (1990). Synaptic excitation of inhibitory cells by single CA3 hippocampal pyramidal cells of the guinea-pig *in vitro*. *J. Physiol.* *428*, 61–77.
- Miles, R., and Wong, R.K.S. (1986). Excitatory synaptic interactions between CA3 neurones in the guinea-pig hippocampus. *J. Physiol.* *373*, 397–418.
- Mosbacher, J., Schoepfer, R., Monyer, H., Burnashev, N., Seeburg, P.H., and Ruppertsberg, J.P. (1994). A molecular determinant for submillisecond desensitization in glutamate receptors. *Science* *266*, 1059–1062.
- Patton, P.E., and McNaughton, B. (1995). Connection matrix of the hippocampal formation. I. The dentate gyrus. *Hippocampus* *5*, 245–286.
- Rall, W. (1967). Distinguishing theoretical synaptic potentials computed for different soma-dendritic distributions of synaptic input. *J. Neurophysiol.* *30*, 1138–1168.
- Reyes, A.D., Rubel, E.W., and Spain, W.J. (1996). In vitro analysis of optimal stimuli for phase-locking and time-delayed modulation of firing in avian nucleus laminaris neurons. *J. Neurosci.* *16*, 993–1007.
- Scharfman, H.E. (1995). Electrophysiological evidence that dentate hilar mossy cells are excitatory and innervate both granule cells and interneurons. *J. Neurophysiol.* *74*, 179–194.
- Shadlen, M.N., and Newsome, W.T. (1994). Noise, neural codes, and cortical organization. *Curr. Opin. Neurobiol.* *4*, 569–579.
- Silver, R.A., Colquhoun, D., Cull-Candy, S.G., and Edmonds, B. (1996). Deactivation and desensitization of non-NMDA receptors in patches and the time course of EPSCs in rat cerebellar granule cells. *J. Physiol.* *493*, 167–173.
- Softky, W. (1994). Sub-millisecond coincidence detection in active dendritic trees. *Neuroscience* *58*, 13–41.
- Spruston, N., and Johnston, D. (1992). Perforated patch-clamp analysis of the passive membrane properties of three classes of hippocampal neurons. *J. Neurophysiol.* *67*, 508–529.
- Stuart, G., and Sakmann, B. (1995). Amplification of EPSPs by axosomatic sodium channels in neocortical pyramidal neurons. *Neuron* *15*, 1065–1076.
- Stuart, G., Spruston, N., Sakmann, B., and Häusser, M. (1997). Action potential initiation and backpropagation in neurons of the mammalian CNS. *Trends Neurosci.* *20*, 125–131.
- Thomson, A.M., Deuchars, J., and West, D.C. (1993). Single axon excitatory postsynaptic potentials in neocortical interneurons exhibit pronounced paired pulse facilitation. *Neuroscience* *54*, 347–360.
- Tong, G., and Jahr, C.E. (1994a). Multivesicular release from excitatory synapses of cultured hippocampal neurons. *Neuron* *12*, 51–59.
- Tong, G., and Jahr, C.E. (1994b). Block of glutamate transporters potentiates postsynaptic excitation. *Neuron* *13*, 1195–1203.
- Traub, R.D., and Miles, R. (1995). Pyramidal cell-to-inhibitory cell spike transduction explicable by active dendritic conductances in inhibitory cell. *J. Comput. Neurosci.* *2*, 291–298.
- Traub, R.D., Whittington, M.A., Stanford, I.M., and Jefferys, J.G.R. (1996). A mechanism for generation of long-range synchronous fast oscillations in the cortex. *Nature* *383*, 621–624.
- Trussell, L.O., Zhang, S., and Raman, I.M. (1993). Desensitization of AMPA receptors upon multiquantal neurotransmitter release. *Neuron* *10*, 1185–1196.
- Wahl, L.M., Pouzat, C., and Stratford, K.J. (1996). Monte Carlo simulation of fast excitatory synaptic transmission at a hippocampal synapse. *J. Neurophysiol.* *75*, 597–608.
- Zhang, S., and Trussell, L.O. (1994a). Voltage-clamp analysis of excitatory synaptic transmission in the avian nucleus magnocellularis. *J. Physiol.* *480*, 123–136.
- Zhang, S., and Trussell, L.O. (1994b). A characterization of excitatory postsynaptic potentials in the avian nucleus magnocellularis. *J. Neurophysiol.* *72*, 705–718.